Supplemental Materials

I. Deformable image registration quality

I.A. Methods and Materials

The registration quality was assessed using Jacobian determinant maps (1;2) and the inverse consistency error (ICE) of the obtained vector fields (3;4).

I.A.1. Jacobian determinant

The absolute value of the Jacobian determinant is a measure of the local volumetric expansion or contraction mediated by the vector field (1). A positive Jacobian further ensures well-behaved, locally invertible transformation fields without cell folding (1) and is therefore frequently used to examine the consistency and quality of registration results (5-8). Jacobian maps of the vector fields were calculated for each transition from the reference phase to all other 4DCT phases, using Plastimatch (9). For each vector field, mean, minimum and maximum Jacobian values within the CTV volume were determined.

I.A.2. Inverse consistency error

Inverse consistency is required for any physical displacement field, i.e., the displacement field obtained for registration of an image A to B needs to be the inverse of the field obtained via registration of image B to A. Real world DIR algorithms, however, in general are not perfectly inverse consistent. Inverse consistency can be quantified using ICE maps which can be thought of as the residual displacement field obtained after catenation of forward and backward transformations: $T(A \rightarrow B) \bullet T(B \rightarrow A)$ (4). We have calculated ICE maps for each pair of phase transitions between the reference phase and the other 4DCT phases using in-house developed software. Since after transformation $T(A \rightarrow B)$ destination positions are in general not on the CT grid, additional tri-linear interpolation among neighboring voxels was employed to determine the subsequent transformation vectors for $T(B \rightarrow A)$. ICE maps were then analyzed for the mean Euclidean norm of the residual displacement vectors and its SD within the CTV. For simplicity, the term ICE will be used synonymously with the norm of the vector in the following.

I.B. Results

Figures 5 and 6 show the results for the Jacobian and ICE as box-and-whisker plots, respectively. Minimum Jacobian values are positive for all patients and vector fields. Mean Jacobians are around 1.0 and maximum Jacobians mostly below 1.5 indicating largely incompressible tissue as expected for the Liver (10).

Mean ICE values of the patients range between 0 and 4 mm with an SD between 0 and 2 mm. As has been shown by Bender et al. (4), the ICE may serve as a lower bound to the true registration accuracy. The obtained spectrum of ICE values is compatible with the average registration accuracy of 4.2 mm (vector magnitude) reported by Brock et al. for the liver with the same registration software (11).

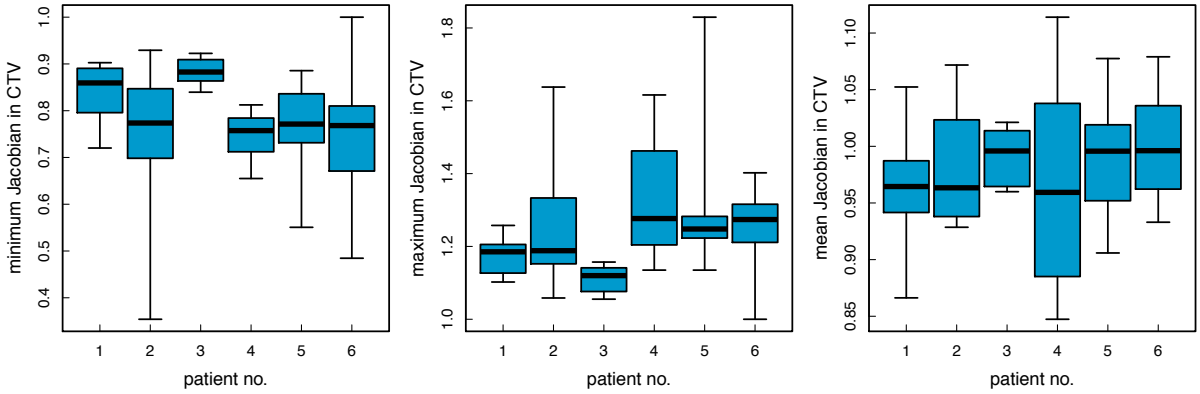

Figure 5: Box-and-whisker plots for the minimum, maximum and mean Jacobian in the CTV for the six patients. Each box plot comprises data points for the respective parameter derived from the vector fields of all 4DCT phase transitions.

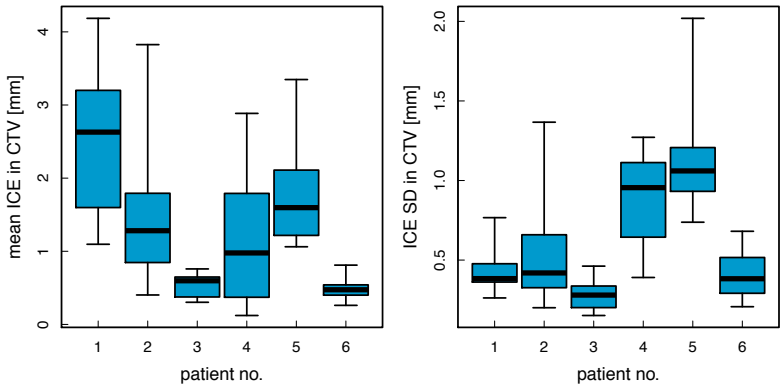

Figure 6: Box-and-whisker plots for the mean ICE and SD in the CTV for the six patients. Each box plot comprises data points for the respective parameter derived from the vector fields of all 4DCT phase transitions.

II. ANZAI delay and stability tests

Data acquisition for dose reconstruction requires a beam status signal, the irradiation time of each raster point and a motion monitoring signal. Furthermore, for all signals sufficient synchronization in time and adequate sampling rates are needed. Delay and stability of the motion signal from the ANZAI system (ANZAI AZ-733V, ANZAI MEDICAL CO., LTD) as a self-contained medical product were determined in a dedicated phantom experiment.

II.A. Methods and materials

II.A.1. New data acquisition system

We use an EtherCAT-based real-time acquisition system (Beckhoff EtherCAT, Beckhoff Automation GmbH, Germany) developed for industrial applications. It provides variable sampling times down to 50 µs (20 kHz rate). This is more than sufficiently fast to record the irradiation times of raster points which are on the order of several milliseconds and potentially short beam gates of below 1 millisecond. As the EtherCAT (EC) system is routinely used for beam and accelerator monitoring at HIT, beam status and raster point irradiation signals are readily available. Synchronized acquisition of the ANZAI signal is facilitated by feeding the motion signal from an analog output port of the ANZAI acquisition device into an analog input of our EC system.

II.A.2. Experimental setup

A commercial motion platform (QUASAR Modus Medical Devices Inc., London, Canada) was used to run a sinusoidal motion pattern at a cycle time of ~5.33 sec. A laboratory laser distance sensor (beta SENSORIK GmbH, Germany) and the ANZAI laser distance sensor were both aligned to independently track the displacement of the platform at close-by positions on a white tape reflector. The lab laser signal was directly fed into an additional analog input of our EC system. The ANZAI laser signal was acquired as described in section II.A.1. Both analog signals were acquired over 30 min with a sampling of 250 µs to determine any signal delays or instabilities of the ANZAI signal with respect to the lab laser signal.

II.A.3. Data analysis

The signal traces each were processed performing two different kinds of fits using a sinusoidal model: (i) a single fit over the full signal range (FR), and (ii) sliding window (SW) fits over parts of the acquisition range. The latter were performed around each of the maxima using a fit range of ± 4 periods. This value was determined as a reasonable compromise between stability and temporal resolution. The iterative fit procedure was performed as follows: In the n^{th} step, the laboratory laser signal was fitted around a time t_L^n close to a maximum at time t_{ML}^n using the sinusoidal model:

$$A(t) = s_L \sin\left(2\pi \frac{t - t_L^n}{T_L} + {}^{\pi}/_{2} + \phi_L\right) + o_L \,.$$

s_L, T_L, ϕ_L and o_L are free parameters. Then, the true maximum of the signal at t_{ML}^n near t_L^n was determined using an iterative maximum search for the optimized model. For the ANZAI signal, an independent fit around t_L^n was performed using an analogous model and yielding the corresponding maximum t_{MA}^n. For the instance n+1 of the SW fit it holds: $t_L^{n+1} = t_{ML}^n + T_L^n$. Pairwise differences $\Delta t^n = t_{MA}^n - t_{ML}^n$ between the maxima were analyzed to determine the phase difference of the signals over time and were checked against the phase differences $\Delta\phi = \phi_A - \phi_L$ obtained from the parameter optimization of SW and FR fits. Signal periods were analyzed via the parameters T_L and T_A from SW and FR fits.

II.B. Results

Time differences Δt of (7012 ± 645) µs were determined by the SW fit corresponding to an average phase delay of about 0.47 degrees of the ANZAI with respect to the lab laser signal. A comparable result of about 0.41 degrees was obtained from $\Delta\phi$ of both the SW and FR fits.

Signal periods determined by the SW fit were very stable for both signals (SD < 10^{-3} %). A systematic difference in the period of (173 ± 27) µs was determined by the SW fits. This difference was not confirmed by the FR fits and is likely to be related to artifacts introduced due to missing continuity and differentiability conditions between individual instances of the SW fit. The FR fit yielded a period of 5.3323 sec for both signals, providing an excellent description of the signals over the whole acquisition time without noticeable drifts.

The small delay of the ANZAI signal is most likely caused by the ANZAI data acquisition system hardware. Our analysis of the dosimetric impact of such a delay with respect to the beam delivery shows that the reconstructed dose distribution will not be significantly affected.

III. Reference List

1. Kaplan W. Differential of Functions of n Variables. The Jacobian Matrix. Advanced Calculus. 5 ed. Boston: Addison-Wesley; 2003. p. 90.

2. Leow AD, Yanovsky I, Chiang MC, et al. Statistical properties of Jacobian maps and the realization of unbiased large-deformation nonlinear image registration. *IEEE Trans Med Imaging* 2007;26:822-32.

3. Leow A, Huang SC, Geng A, et al. Inverse consistent mapping in 3D deformable image registration: its construction and statistical properties. *Inf Process Med Imaging* 2005;19:493-503.

4. Bender ET, Tome WA. The utilization of consistency metrics for error analysis in deformable image registration. *Phys Med Biol* 2009;54:5561-77.

5. Sarkar S, Johnson TD, Ma B, et al. Evaluation of an automatic registration-based algorithm for direct measurement of volume change in tumors. *Int J Radiat Oncol Biol Phys* 2012;83:1038-46.

6. Varadhan R, Karangelis G, Krishnan K, et al. A framework for deformable image registration validation in radiotherapy clinical applications. *J Appl Clin Med Phys* 2013;14:4066.

7. Vercauteren T, De GW, Olteanu LA, et al. Deformation field validation and inversion applied to adaptive radiation therapy. *Phys Med Biol* 2013;58:5269-86.

8. Kim J, Kumar S, Liu C, et al. A novel approach for establishing benchmark CBCT/CT deformable image registrations in prostate cancer radiotherapy. *Phys Med Biol* 2013;58:8077-97.

9. Shackleford JA, Kandasamy N, Sharp GC. On developing B-spline registration algorithms for multi-core processors. *Phys Med Biol* 2010;55:6329-51.

10. Hinkle J, Szegedi M, Wang B, et al. 4D CT image reconstruction with diffeomorphic motion model. *Med Image Anal* 2012;16:1307-16.

11. Brock KK. Results of a multi-institution deformable registration accuracy study (MIDRAS). *Int J Radiat Oncol Biol Phys* 2010;76:583-96.